Droplet-superfluid compounds in binary bosonic mixtures

M. Nilsson Tengstrand* and S. M. Reimann
Division of Mathematical Physics and NanoLund, Lund University, SE-221 00 Lund, Sweden

(Received 5 November 2021; accepted 8 March 2022; published 24 March 2022)

While quantum fluctuations in binary mixtures of bosonic atoms with short-range interactions can lead to the formation of a self-bound droplet, for equal intracomponent interactions but an unequal number of atoms in the two components, there is an excess part that cannot bind to the droplet. Imposing confinement, as here through periodic boundary conditions in a one-dimensional setting, the droplet becomes amalgamated with a residual condensate. The rotational properties of this compound system reveal simultaneous rigid-body and superfluid behavior in the ground state and uncover that the residual condensate can carry angular momentum even in the absence of vorticity. In contradiction to the intuitive idea that the superfluid fraction of the system would be entirely made up of the excess atoms not bound by the droplet, we find evidence that this fraction is higher than what one would expect in such a picture. Our findings are corroborated by an analysis of the elementary excitations in the system, and shed new light on the coexistence of localization and superfluidity.

DOI: 10.1103/PhysRevA.105.033319

I. INTRODUCTION

In the field of ultracold atomic quantum gases it was suggested early on [1–3] that quantum effects beyond mean field (BMF) may lead to self-bound droplets of fermionic or bosonic atoms. For weakly interacting single-component Bose gases, quantum fluctuations are often too small to play any significant role. Nevertheless, for binary or dipolar Bose gases the interactions may be adjusted such that the different main contributions to the mean-field (MF) energy nearly cancel out, leaving only a small residual term that can be tuned to equilibrate with the BMF part of the total energy. A self-bound dilute boson droplet may then form [4,5], with curious properties originating from its genuine quantum many-body nature. Although originally proposed for binary Bose gases [5], the first experimental observations of droplets stabilized by the Lee-Huang-Yang (LHY) quantum fluctuations [6] were made for dipolar atoms, dysprosium [7–10] and erbium [11]. Here, a scenario similar to the binary case [12] arises due to the peculiarities of the dipolar interactions [13–17]. Experiments with binary bosonic mixtures of potassium [18–20] or heteronuclear mixtures [21,22] followed soon after (see the reviews [23,24]). In low-dimensional systems, quantum fluctuations may be enhanced, facilitating and stabilizing the droplet formation process [5,25,26], and the dimensional crossover has been discussed in Refs. [27–29]. Recent work on binary self-bound states in one dimension (1D) or quasi-1D also investigated corrections beyond LHY [30], applied the quantum Monte Carlo method [26,31], used the Bose-Hubbard model [32,33] or formulated an effective quantum field theory [34]. It has been shown that microscopic pairing or dimer models agree with variational approaches [35,36]. Collective excitations [37,38] and thermodynamic properties [30,39] were also studied.

Droplets may also form in systems with intercomponent asymmetry. One obvious realization is heteronuclear mixtures, see, e.g., Refs. [21,22,40–42]. Another interesting scenario arises when the intracomponent interactions are equal, but the components have different particle numbers. Then, the excess particles in the larger component cannot bind to the droplet [4], but instead form a uniform background into which the droplet is immersed [43]. Another interesting scenario can occur for nonequal intraspecies interactions around the miscibility-immiscibility threshold, where it was recently suggested [44] that a mixed phase may coexist with a nonamalgamated gaseous component, where partial miscibility is caused by BMF contributions leading to bubble phases.

In this paper, we set focus on the case of asymmetric components confined in a one-dimensional trap with periodic boundary conditions. For equal intraspecies interactions but different numbers of particles in the two components, with increasing coupling strength the translational symmetry of the uniform system is broken. A localized droplet forms, stabilized by quantum fluctuations, which coexists with a uniform residual condensate of excess atoms that cannot bind to the droplet, but are kept together by the confinement. We demonstrate that this asymmetric system, although with just a single droplet unlike what is typically seen in dipolar supersolids [23], simultaneously exhibits rigid-body and superfluid properties. The nonclassical rotational inertia (NCRI) reveals that the motion of the droplet at low velocities is not only that of a classical rigid body but is accompanied by the response of the nondroplet atoms moving in a direction opposite to the motion

*mikael.nilsson_tengstrand@matfys.lth.se

of the rigid body. Importantly, this response is found to exist for infinitesimal rotations, thus having a profound impact on the degree of superfluidity of the system. The number of atoms contributing to the formation of a vortex is larger than that of the residual condensate, coinciding with the NCRI fraction. Our findings are corroborated by an analysis of the lowest excitation modes in the compound system.

II. MODEL AND METHODS

The energy density for a uniform binary Bose-Bose mixture in one dimension with equal masses and short-ranged interactions, including BMF corrections, equals [5]

$$\mathcal{E} = \frac{g}{2}(n_2 - n_1)^2 + \delta g n_1 n_2 - \frac{2m^{1/2}g^{3/2}}{3\pi\hbar}(n_1 + n_2)^{3/2}, \quad (1)$$

where n_i are the densities of each component and m the mass of a single particle. Here we have set the intraspecies coupling constants to be equal, $g_{11} = g_{22} = g$, and introduced $\delta g = g + g_{12}$, where g_{12} is the interspecies coupling constant. The first two terms in Eq. (1) constitute the MF energy density and the last term accounts for the first correction beyond mean field. The energy density Eq. (1) is valid provided $\eta = \sqrt{mg/n\hbar^2} \ll 1$, ensuring weak interactions (here we have assumed similar order of magnitudes for the densities $n_1 \sim n_2 \sim n$), and that δg is small in the sense $\delta g/g \sim \eta$. For a finite-size system the extended coupled Gross-Pitaevskii equations corresponding to the energy density Eq. (1) are

$$\begin{aligned} i\hbar\partial_t\psi_i = &-\frac{\hbar^2}{2m}\partial_{xx}\psi_i + g|\psi_i|^2\psi_i + (\delta g - g)|\psi_j|^2\psi_i \\ &- \frac{m^{1/2}g^{3/2}}{\pi\hbar}(|\psi_i|^2 + |\psi_j|^2)^{1/2}\psi_i, \end{aligned} \quad (2)$$

where $i, j = 1, 2$ and $i \neq j$. We impose periodic boundary conditions $\psi_i(x) = \psi_i(x + 2\pi R)$, enforcing a confinement of length $2\pi R$. This is a good approximation for a ring of radius R [45,46] whenever bending effects may be neglected, i.e., when the transversal confinement length is much smaller than R. Such binary one-dimensional ring systems have been extensively studied, both experimentally [47–54] and theoretically [55–65]. We note that the validity of using a position-dependent beyond-mean-field contribution can be motivated on the basis of the semiclassical approximation (for a background motivating this statement, see, e.g., Refs. [13,14,66–69]).

From here on, we use dimensionless units such that $\hbar = m = R = 1$. The order parameter is normalized to the number of particles in each component, $\int_0^{2\pi} |\psi_i(x)|^2 dx = N_i$. The ground state is obtained by solving Eq. (2) numerically with a split-step Fourier method in imaginary time. To analyze the system in a rotating frame the term $-\Omega\hat{L}\psi_i$ is added to the right side of Eq. (2), where $\hat{L} = -i\partial_x$, which is then solved in the same manner. In order to find the ground state for a fixed value of the angular momentum $L = L_1 + L_2$, where $L_i = \int_0^{2\pi} \psi_i^*\hat{L}\psi_i dx$, we consider the quantity $\tilde{E} = E + (C/2)(L - L_0)^2$ [70–73], where E is the total energy corresponding to Eq. (2). By minimizing $\tilde{E}$ for sufficiently large values of the constant $C > 0$, the obtained ground state will have angular momentum $L \approx L_0$ since the critical point of $\tilde{E}$ is $L = L_0 - \partial_L E/C$, which is a minimum whenever $C > -\partial_{LL}E$. Introducing $\lambda = \delta g/g$, $N = N_1 + N_2$ and $\nu = N_2/N_1$, we illustrate our findings below by fixing $\lambda = 0.01$ and $N = 5000$. The asymmetry parameter is restricted to $\nu \geqslant 1$.

In order to study the spectrum of elementary excitations (see Sec. IV), we linearize Eq. (2) around the ground state $\psi_{0,i}$ by writing

$$\psi_i(x,t) = e^{-i\mu_i t}[\psi_{0,i}(x) + u_i(x)e^{-i\omega t} + v_i^*(x)e^{i\omega^* t}] \quad (3)$$

and keeping terms up to first order in the Bogoliubov amplitudes u_i and v_i. Here μ_i is the chemical potential and $\omega/2\pi$ the frequency of oscillation of u and v. Due to the periodicity of the system we expand the amplitudes in plane waves $u_i(x) = e^{ikx}u_{i,k}(x)$ and $v_i(x) = e^{ikx}v_{i,k}(x)$, resulting in the Bogoliubov–de Gennes equations

$$\mathbf{A}_k\mathbf{v}_k = \omega_k\mathbf{v}_k, \quad (4)$$

where $\mathbf{v}_k = (u_{1,k}(x) \quad v_{1,k}(x) \quad u_{2,k}(x) \quad v_{2,k}(x))^{\mathrm{T}}$ and

$$\mathbf{A}_k = \begin{pmatrix} X_{12,k} & Y_1 & Z & Z \\ -Y_1 & -X_{12,k} & -Z & -Z \\ Z & Z & X_{21,k} & Y_2 \\ -Z & -Z & -Y_2 & -X_{21,k} \end{pmatrix} \quad (5)$$

with

$$\begin{aligned} X_{ij,k} &= -\frac{1}{2}\frac{\partial^2}{\partial x^2} - ik\frac{\partial}{\partial x} + \frac{k^2}{2} - \mu_i \\ &\quad + (2g - 3\alpha)\psi_{0,i}^2 + (\delta g - g - 2\alpha)\psi_{0,j}^2 \\ Y_i &= (g - \alpha)\psi_{0,i}^2 \\ Z &= (\delta g - g - \alpha)\psi_{0,1}\psi_{0,2} \end{aligned} \quad (6)$$

and

$$\alpha = \frac{g^{3/2}}{2\pi\left(\psi_{0,1}^2 + \psi_{0,2}^2\right)^{1/2}}. \quad (7)$$

Here α is the contribution due to beyond mean-field effects and we have assumed $\psi_{0,i}$ to be real. We solve Eq. (4) numerically with standard diagonalization techniques.

III. GROUND-STATE PROPERTIES

We first investigate the density distributions of the two components, starting with the symmetric case where both components of the mixture are equal, $\nu = 1$. The top panel of Fig. 1 shows the corresponding densities for different values of the interaction parameter g for a slowly rotating system. For high enough values of g the ground state has the form of a droplet in agreement with previous findings in one dimension [5,25]. As g is decreased the extent of the droplet increases, which results in a transition to a uniform state. We understand this by considering the bulk density of a flat-top droplet $n_0 = 8g/(9\pi^2\lambda^2)$ [5], which implies a droplet extent $\sim N/(2n_0)$. When this droplet size is much smaller than the ring length the periodic boundary conditions do not significantly affect the system. As g is decreased, the droplet size eventually becomes comparable to the ring length for $g \sim 9\pi N\lambda^2/32$. This results in a transition from a droplet to a uniform system and is a consequence of the periodic boundary conditions. (See also the discussion of boundary effects in Ref. [74].) For

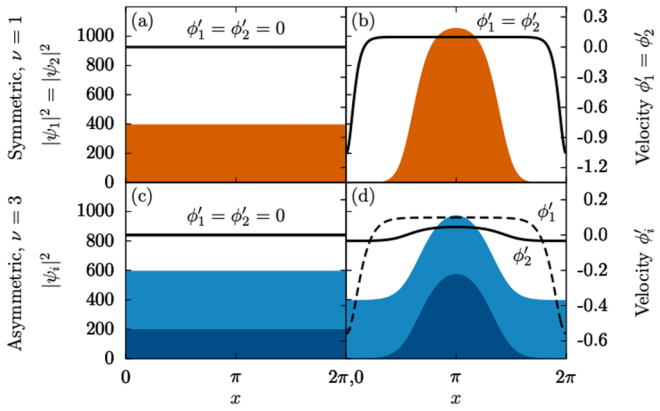

FIG. 1. Densities $|\Psi_i|^2$ (red, blue) and velocities ϕ_i' (black lines) of the two components in the rotating frame where $N = 5000$, $\delta g/g = 0.01$, and $\Omega = 0.1$. The top panel shows the symmetric case, $\nu = 1$. (a) $|\Psi_1|^2 = |\Psi_2|^2$ for $g = 0.5$ (red), being homogeneous along the ring. (b) as in (a) but for $g = 1.2$, showing droplet formation. The bottom panel shows the asymmetric case for $\nu = 3$ for the same parameters as in the top panel. The axis to the right in both panels shows the corresponding condensate velocities ϕ_i'. Units are dimensionless.

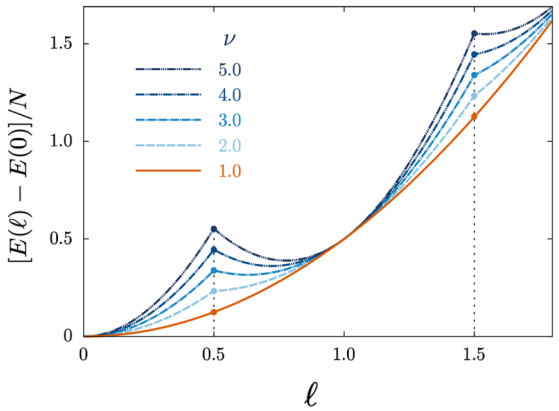

FIG. 2. Energy as a function of angular momentum per particle for $\nu = 1, \ldots, 5$ (see legend), $g = 1.5$. Units are dimensionless.

low values of g, the situation is similar also in the asymmetric case, where both components display uniform behavior, as shown for $\nu = 3$ in the bottom panel of Fig. 1.

With increasing interaction strength g the translation symmetry is eventually broken, and the ground-state density for the component with more particles changes to what appears to be a mix between a droplet and a uniform medium, while the other component displays a normal droplet solution. The droplet coexists with a uniform background, since the excess particles in the second component can not bind to it [4]. Deviating from $\nu = 1$ results in an increase in the ratio of MF to BMF energy, eventually causing the former to dominate the total energy. Thus, unlike the symmetric case where droplet formation takes place where the MF and BMF terms are of similar orders of magnitude, for the asymmetric system we have BMF effects such as displayed in Fig. 1 even though the MF contribution can be much larger than the BMF one. If Eq. (2) is solved without the BMF contribution *ceteris paribus* we find uniform solutions in the regimes where nonuniform ones were obtained with the full Eq. (2) for our choice of parameters. We can understand this by considering the interaction energy density Eq. (1), where for sufficiently large ν the first term is the dominant one and the second and third terms are of order η. In the homogeneous regime the densities are simply $n_i = N_i/(2\pi)$ and the energy corresponding to the first term (in dimensionless units) is thus $g(N_2 - N_1)^2/(4\pi)$. In the droplet regime we see from Fig. 1 that the densities take the form $n_1(x) = n_d(x)$ and $n_2 = n_d(x) + (N_2 - N_1)/(2\pi)$, where $n_d(x)$ is the density of the droplet part. Since $n_2(x) - n_1(x) = (N_2 - N_1)/(2\pi)$ we find that the energy corresponding to the dominant first term must be the same in the uniform and droplet regimes, and the ground state is consequently determined by the interplay between the small part of the mean-field contribution $\delta g n_1 n_2$ and the beyond-mean-field correction, just as for the symmetric system.

We are here interested in the properties of the mixed-phase system. The ground-state energy $E(\ell)$ as a function of the angular momentum per particle $\ell \equiv (L_1 + L_2)/N$, where L_i is the angular momentum of component i as defined in Sec. II, is shown in Fig. 2 for different degrees of asymmetry ν. It takes the form of a single parabola for $\nu = 1$, corresponding to the rigid-body rotation of the droplet in the ring. For the asymmetric case with $\nu > 1$, different parabolas appear to intersect. Intriguingly, the structure of $E(\ell)$ is similar to the one found for a three-dimensional dipolar toroidal system in the supersolid phase [75]. With this analogy in mind, we model the system by considering N_c particles taking angular momentum as a classical rigid body under rotation and N_v particles taking angular momentum only in terms of vorticity, with $N = N_c + N_v$. The energy cost for adding a vortex with s-fold quantization to the condensate can be determined by assuming an order parameter for the vortex component on the form $\propto e^{isx}$, where the integer s is the angular momentum per particle in the vortex-carrying component, leading to an energy cost equal to $N_v s^2/2$. Since the solidlike part of the system carries angular momentum according to $N_c \ell_c^2/2$, where ℓ_c is its angular momentum per particle and $N\ell = N_c \ell_c + N_v s$, the different energetic branches dependent on angular momentum can be written

$$E_s/N = \frac{1}{2}\left[\frac{(\ell - f_v s)^2}{1 - f_v} + f_v s^2\right], \tag{8}$$

where we have defined the fraction of particles carrying vorticity $f_v = N_v/N$. The branches E_s and E_{s+1} intersect at $\ell = s + 1/2$, i.e., having no vortex is energetically favorable for $\ell < 0.5$, having a singly quantized one for $0.5 < \ell < 1.5$ and so on. The energies in Eq. (8) obtained within our model predict that the functional form of the dispersion relation should be parabolas intersecting at half-integer values of ℓ, in accordance with the numerical results displayed in Fig. 2.

Importantly, this suggests that the asymmetric system can exhibit properties of a solid and superfluid simultaneously, with rigid-body rotation and quantized vorticity coexisting. Unlike ring-shaped dipolar supersolids, which display a similar behavior under rotation [75,76], here in the case of isotropic short-range interactions the ground-state density does not exhibit any repeating crystalline structure. Since the

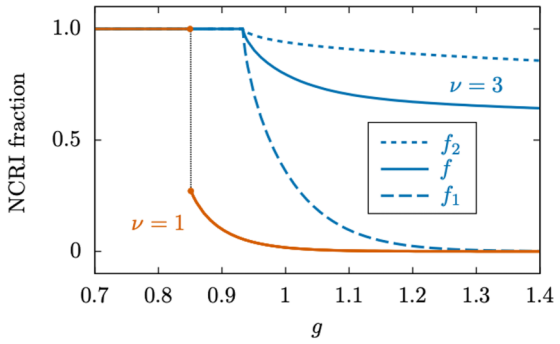

FIG. 3. Nonclassical rotational inertia (NCRI) fraction as a function of interaction strength g for $\nu = 1$ (orange; the discontinuity is indicated by the bullets and connecting dashed line), and for $\nu = 3$ with f_1, f_2, and f as indicated in the legend. (Note that $f = f_1 = f_2$ for the symmetric system). Units are dimensionless.

branches E_s have minima at $\ell = f_v s$, there is a possibility for the system to exhibit metastable superflow. These minima exist in the ground-state energy $E(\ell)$ only if they occur on the interval where the corresponding branch $E_s(\ell)$ is the lowest in energy, thus giving a criterion for the existence of a metastable persistent current related to an s times multiply quantized vortex according to $f_v > (2s-1)/(2s)$.

It is tempting to identify the amount of particles belonging to the vortex component with the number $N_2 - N_1$, intuitively imagining that N_1 particles from each component bind as a droplet and thus act in a solid-body fashion while the excess particles take the role of a background superfluid capable of carrying vorticity. If this were true, then $f_v = (N_2 - N_1)/N = (\nu-1)/(\nu+1)$, in contradiction with the numerically obtained positions of the minima in Fig. 2, which were predicted to occur at $\ell = f_v s$. To give an example, for $\nu = 3$ the first minimum occurs at $\ell \approx 0.63$ while $(\nu-1)/(\nu+1) = 0.5$. To investigate this obvious discrepancy, we compute the nonclassical rotational inertia fraction for each component [77,78]

$$f_i = 1 - \lim_{\Omega\to 0} \frac{L_i}{N_i \Omega}. \tag{9}$$

The total NCRI fraction is defined as $f = (N_1 f_1 + N_2 f_2)/N$, and we plot the numerically obtained results in Fig. 3 for $\nu = 1$ and $\nu = 3$. Interestingly, for $\nu = 1$ there is a discontinuous jump from $f = 1$ to a value that is nonzero, signaling that even for the symmetric droplet system there are parameter values such that the motion is not entirely classical. As ν is increased the discontinuity decreases until it eventually disappears, as exemplified for $\nu = 3$ in Fig. 3. We see that the total NCRI fraction for the asymmetric system not only differs from $(\nu-1)/(\nu+1)$ but is also dependent on g.

Let us now study the motion of the condensate under rotation by examining the condensate velocity. We start by considering the time-independent coupled extended Gross-Pitaevskii equations in the rotating frame

$$\begin{aligned}\mu_i\psi_i = &-\frac{1}{2}\psi_i'' + g|\psi_i|^2\psi_i + (\delta g - g)|\psi_j|^2\psi_i \\ &- \frac{g^{3/2}}{\pi}(|\psi_i|^2 + |\psi_j|^2)^{1/2}\psi_i - \Omega\hat{L}\psi_i,\end{aligned} \tag{10}$$

where it is assumed that $i \neq j$ as before. Writing $\psi_i(x) = \tilde{\psi}_i(x)e^{i\phi_i(x)}$ and inserting into Eq. (10) we find

$$\begin{aligned}\mu_i\tilde{\psi}_i = &-\frac{1}{2}\tilde{\psi}_i'' + \frac{1}{2}\tilde{\psi}_i(\phi_i')^2 + g\tilde{\psi}_i^3 + (\delta g - g)\tilde{\psi}_j^2\tilde{\psi}_i \\ &- \frac{g^{3/2}}{\pi}\left(\tilde{\psi}_i^2 + \tilde{\psi}_j^2\right)^{1/2}\psi_i - \Omega\tilde{\psi}_i\phi_i' \\ &+ i\left(-\tilde{\psi}_i'\phi_i' - \frac{1}{2}\tilde{\psi}_i\phi_i'' + \Omega\tilde{\psi}_i'\right).\end{aligned} \tag{11}$$

Using the fact that $\tilde{\psi}_i$ and ϕ_i are real we separate Eq. (11) into two equations by identifying real and imaginary terms, where the imaginary part yields the equation

$$\tfrac{1}{2}\tilde{\psi}_i\phi_i'' + \tilde{\psi}_i'\phi_i' = \Omega\tilde{\psi}_i'. \tag{12}$$

This equation can be solved for the condensate velocity $\phi_i'(x)$ in terms of $\tilde{\psi}_i(x)$, with the solution

$$\phi_i'(x) = \Omega + \frac{C_i}{n_i(x)}, \tag{13}$$

where C_i is an integration constant and $n_i = |\psi_i|^2 = \tilde{\psi}_i^2$. Since the angular momentum can be written $L_i = \int n_i(x)\phi_i'(x)dx$ we finally obtain an expression for the velocity

$$\phi_i'(x) = \Omega + \frac{L_i - N_i\Omega}{2\pi n_i(x)}. \tag{14}$$

The velocities for some parameters are plotted in Fig. 1 where in particular Figs. 1(b) and 1(d) show how the velocity for both components in the symmetric system and the first component in the asymmetric one are equal to Ω throughout most of the ring, reflecting the solidlike movement. Away from the bulk of the droplet where the density is small, the second term in Eq. (14) becomes significant and the velocity thus deviates from Ω in a manner depending on $L_i - N_i\Omega$. For small Ω this difference is negative, resulting in a change of sign for the velocity as displayed in Figs. 1(b) and 1(d). If the density is negligible in the region where the velocity deviates from Ω this will have little effect, but if the droplet instead occupies most of the ring, as is the case close to the transition point between the uniform and droplet phases, this results in parts of the system moving in a direction opposite to the rest of the condensate. The NCRI fraction will consequently differ from zero, explaining why f for the symmetric system and f_1 for the asymmetric system do not immediately fall to zero at the transition point. For the second component in the nonuniform asymmetric case the velocity has opposite signs inside and outside the droplet region, indicating that the movement of the droplet is accompanied by a response of the background medium, which moves in the other direction. Since this response exists also for infinitesimal rotations, it affects the results based on the definition in Eq. (9), increasing it compared to if there had been no response flow of the background. Curiously, this implies that the interpretation of f as the fraction of particles that stay at rest as the container is set to slowly rotate is not a correct one. (Interestingly, a similar type of response by the background has been noticed also for dipolar condensates in the supersolid phase [75,79].) To connect to the results in Fig. 2, we compute the corresponding NCRI fractions and find that $f \approx 0.47$, $f \approx 0.63$, $f \approx 0.72$,

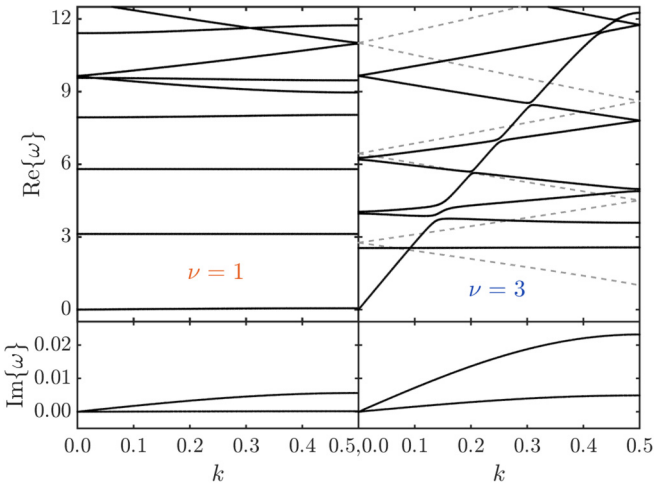

FIG. 4. Spectra of elementary excitations for $\nu = 1$ (left) and $\nu = 3$ (right) as a function of k for $g = 1.4$ where the top panels show the real modes and the bottom panels the imaginary modes. The (gray) dashed lines show the analytical solutions in the homogeneous regime for $|p| \geqslant 3$ (see text) for the corresponding parameter values. Note that the y axes to the left also apply to the panels of the right column. Units are dimensionless.

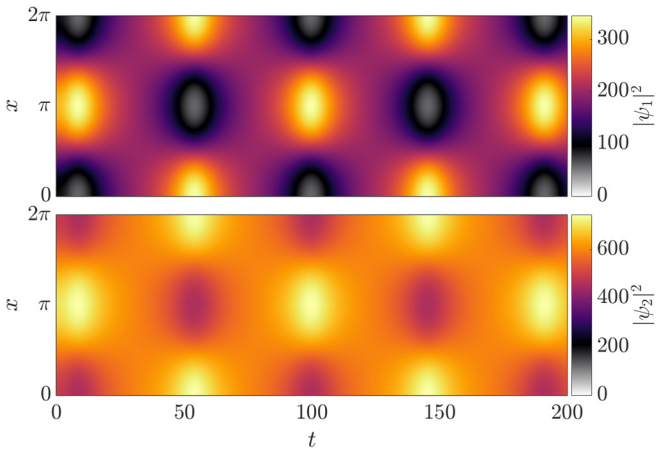

FIG. 5. Real-time evolution of the ground-state densities for an asymmetric system with $\nu = 3$ and $g = 0.94$ close to the phase boundary. At $t = 0$ the interaction strength is suddenly changed to $g = 0.95$, which is then turned back to $g = 0.94$ at $t = 5$ (keeping λ constant). The top panel shows the evolution of the first component and the bottom panel the evolution of the second component. Note that the x axis at the bottom applies to both panels. Units are dimensionless.

and $f \approx 0.78$ for $\nu = 2, 3, 4, 5$, respectively. These data agree well with the positions of the minima of $E(\ell)$, suggesting that $f_v \approx f$ for these asymmetric systems, i.e., that the fraction of particles related to vortex formation is larger than that of the residual condensate and coincides with the NCRI fraction. We note that the energy as a function of angular momentum for the symmetric case $\nu = 1$ always takes the form of a single parabola as displayed in Fig. 2, even when the NCRI fraction is different from zero but smaller than one (i.e., around the transition point $g \approx 0.85$ in Fig. 3). This indicates that for $\nu = 1$ we may have $f \neq f_v = 0$ and that the fraction of residual condensate needs to be nonzero for the vortex fraction to also be nonzero.

IV. EXCITATION SPECTRUM

Finally, we investigate the spectra of collective excitations by solving Eq. (4) numerically. Figure 4 shows the lowest modes as a function of k for the symmetric ($\nu = 1$) and asymmetric case (here for $\nu = 3$) in the nonuniform regime.

In both cases there are three modes that are gapless at $k = 0$. Two of these are purely imaginary (see the bottom panels in Fig. 4) and one is purely real. Imaginary solutions indicate a dynamical instability of the system (see, for example, Refs. [80–82]), and we find that when g is decreased and we approach the uniform regime these imaginary modes harden, implying a higher degree of instability closer to the phase boundary. With increased g the modes instead soften until they become vanishingly small and the system thus becomes stable. The hardening of the imaginary modes as g is decreased towards the phase boundary suggests that the instability in the nonuniform phase originates from the periodic boundary conditions, and we investigate this further by means of real-time propagation. We consider a situation where the interaction strength g is at $t = 0$ suddenly changed to a slightly higher value for a short time and then turned back to its original value (while keeping λ constant at all times). As an example, Fig. 5 shows the real-time evolution of a droplet-superfluid compound close to the phase boundary for $\nu = 3$ and $g = 0.94$ when it is excited in this way. It can be seen how the droplet continuously collapses and is reformed at a position displaced by π compared to the previous droplet location. Furthermore, we find that the closer we are to the phase boundary the smaller the perturbation has to be to bring about such a recurring droplet collapse. Notably, we do not find similarly unstable behavior by perturbing a uniform system close to the phase boundary (which has no imaginary modes), where the density oscillations instead are very small, something that is true also deeper in the droplet regime for large values of g. We thus find these mixtures with periodic boundary conditions to be dynamically stable under this type of small perturbations except close to the phase boundary from the nonuniform side, in accordance with results for the excitation spectra.

We find that the real mode that is gapless at $k = 0$ is tied to the superfluidity of the system. For the symmetric case, it becomes soft rapidly as the NCRI goes to zero, see the lowest mode in the top left panel in Fig. 4. With increasing ν the superfluid character of the condensate is enhanced, hardening this mode such that it for $k > 0$ may result in crossings and avoided crossings with the higher modes, see the top right panel of Fig. 4. The lowest-lying modes of the pure droplet system that are nonzero at $k = 0$ are characterized by their insensitivity to changes in k, the first one being the breathing mode [38]. For the asymmetric system we find by studying the Bogoliubov amplitudes that the lowest nonzero at $k = 0$ mode is still the breathing mode, followed by higher modes with linear slopes that form a zigzag pattern higher up in the spectrum. We can understand this structure from the solution of the Bogoliubov–de Gennes equations of the uniform condensate,

which may be obtained analytically through the ansatz [83]

$$\mathbf{v}_k(x) = \sum_{p=-\infty}^{\infty} \frac{e^{ipx}}{\sqrt{2\pi}} \tilde{\mathbf{v}}_{pk}, \tag{15}$$

where $\tilde{\mathbf{v}}_{pk} = (\tilde{u}_{1,pk} \quad \tilde{v}_{1,pk} \quad \tilde{u}_{2,pk} \quad \tilde{v}_{2,pk})^{\mathrm{T}}$. By substituting into Eq. (4) we readily find the solutions

$$\omega^2_{\pm,pk} = \frac{(p+k)^2}{4\pi}[\pi(p+k)^2 + (g-\alpha)N \pm\sqrt{(g-\alpha)^2(N_1-N_2)^2 + 4(\delta g - g - \alpha)^2 N_1 N_2}], \tag{16}$$

which in the limit $g \gg \delta g, \alpha$ can be written as

$$\omega^2_{+,pk} \approx \frac{(p+k)^2}{4\pi}\left[\pi(p+k)^2 + 2(g-\alpha)N - 4(\delta g - 2\alpha)\frac{N_1 N_2}{N}\right] \tag{17}$$

and

$$\omega^2_{-,pk} \approx \frac{(p+k)^2}{4\pi}\left[\pi(p+k)^2 + 4(\delta g - 2\alpha)\frac{N_1 N_2}{N}\right]. \tag{18}$$

From these two types of solutions we observe that there is a separation of scales, where the low-lying part of the spectrum is dominated by the $\omega_{-,pk}$ branches. For sufficiently large $|p|$, $k \in [0.0, 0.5]$ and $\omega_{-,pk} > 0$, we find that the solutions Eq. (18) take the approximate form

$$\omega_{-,pk} \approx \frac{p^2}{2} + pk + (\delta g - 2\alpha)\frac{N_1 N_2}{\pi N},$$

which on the interval $k \in [0.0, 0.5]$ takes the form of a zigzag pattern as displayed in Fig. 4, where it can be seen how the nonuniform system exhibits a structure that is similar to the uniform one, but displaced to higher energies. This is a clear indication for the increased importance of the nondroplet superfluid background higher up in the excitation spectrum.

V. CONCLUSIONS

In summary, we investigated the effects of quantum fluctuations beyond just droplet formation of a binary Bose mixture with short-range interactions in a one-dimensional confinement with periodic boundary conditions. Although the BMF contribution for asymmetric configurations may be small compared to the MF one, it can cause a breaking of translational symmetry. Examining the rotational properties and collective excitations of an asymmetric compound system where a single droplet amalgamates with a residual condensate, we found that rigid-body and superfluid characteristics coexist. The nonclassical rotational inertia (NCRI) revealed that the motion of the droplet at low velocities is not only that of a classical rigid body, but is accompanied by the response of the residual superfluid moving in the opposite direction. This response profoundly impacts on the superfluid fraction as it is also found for infinitesimal rotations. Investigating the collective excitations revealed the existence of a single real gapless phase mode that softens with decreased NCRI, tying it to the degree of superfluidity of the system.

Our findings are expected to hold also in the quasi-one-dimensional limit for a sufficiently strong transversal trapping. As mentioned above, droplets were observed for binary ^{39}K [18–20] or heteronuclear mixtures [21,22]. Anharmonic traps with long-lifetime annular flow [84] and widely tunable ring traps [85] were recently realized, making experiments on toroidal droplet-superfluid compounds a realistic endeavor.

ACKNOWLEDGMENTS

This research was supported by the Knut and Alice Wallenberg Foundation (Projects No. 2016.0089 and No. 2018.0217), and the Swedish Research Council.

[1] A. Bulgac, Phys. Rev. Lett. **89**, 050402 (2002).
[2] P. F. Bedaque, A. Bulgac, and G. Rupak, Phys. Rev. A **68**, 033606 (2003).
[3] H.-W. Hammer and D. T. Son, Phys. Rev. Lett. **93**, 250408 (2004).
[4] D. S. Petrov, Phys. Rev. Lett. **115**, 155302 (2015).
[5] D. S. Petrov and G. E. Astrakharchik, Phys. Rev. Lett. **117**, 100401 (2016).
[6] T. D. Lee, K. Huang, and C. N. Yang, Phys. Rev. **106**, 1135 (1957).
[7] H. Kadau, M. Schmitt, M. Wenzel, C. Wink, T. Maier, I. Ferrier-Barbut, and T. Pfau, Nature (London) **530**, 194 (2016).
[8] I. Ferrier-Barbut, H. Kadau, M. Schmitt, M. Wenzel, and T. Pfau, Phys. Rev. Lett. **116**, 215301 (2016).
[9] I. Ferrier-Barbut, M. Schmitt, M. Wenzel, H. Kadau, and T. Pfau, J. Phys. B: At. Mol. Opt. Phys. **49**, 214004 (2016).
[10] M. Schmitt, M. Wenzel, F. Böttcher, I. Ferrier-Barbut, and T. Pfau, Nature (London) **539**, 259 (2016).
[11] L. Chomaz, S. Baier, D. Petter, M. J. Mark, F. Wächtler, L. Santos, and F. Ferlaino, Phys. Rev. X **6**, 041039 (2016).
[12] C. Staudinger, F. Mazzanti, and R. E. Zillich, Phys. Rev. A **98**, 023633 (2018).
[13] F. Wächtler and L. Santos, Phys. Rev. A **94**, 043618 (2016).
[14] F. Wächtler and L. Santos, Phys. Rev. A **93**, 061603(R) (2016).
[15] A. Macia, J. Sánchez-Baena, J. Boronat, and F. Mazzanti, Phys. Rev. Lett. **117**, 205301 (2016).
[16] R. N. Bisset, R. M. Wilson, D. Baillie, and P. B. Blakie, Phys. Rev. A **94**, 033619 (2016).
[17] D. Baillie, R. M. Wilson, and P. B. Blakie, Phys. Rev. Lett. **119**, 255302 (2017).
[18] C. R. Cabrera, L. Tanzi, J. Sanz, B. Naylor, P. Thomas, P. Cheiney, and L. Tarruell, Science **359**, 301 (2018).
[19] G. Semeghini, G. Ferioli, L. Masi, C. Mazzinghi, L. Wolswijk, F. Minardi, M. Modugno, G. Modugno, M. Inguscio, and M. Fattori, Phys. Rev. Lett. **120**, 235301 (2018).

[20] P. Cheiney, C. R. Cabrera, J. Sanz, B. Naylor, L. Tanzi, and L. Tarruell, Phys. Rev. Lett. **120**, 135301 (2018).

[21] C. D'Errico, A. Burchianti, M. Prevedelli, L. Salasnich, F. Ancilotto, M. Modugno, F. Minardi, and C. Fort, Phys. Rev. Research **1**, 033155 (2019).

[22] Z. Guo, F. Jia, L. Li, Y. Ma, J. M. Hutson, X. Cui, and D. Wang, Phys. Rev. Research **3**, 033247 (2021).

[23] F. Böttcher, J.-N. Schmidt, J. Hertkorn, K. S. H. Ng, S. D. Graham, M. Guo, T. Langen, and T. Pfau, Rep. Prog. Phys. **84**, 012403 (2021).

[24] Z.-H. Luo, W. Pang, B. Liu, Y.-Y. Li, and B. A. Malomed, Front. Phys. **16**, 32201 (2021).

[25] G. E. Astrakharchik and B. A. Malomed, Phys. Rev. A **98**, 013631 (2018).

[26] L. Parisi, G. E. Astrakharchik, and S. Giorgini, Phys. Rev. Lett. **122**, 105302 (2019).

[27] P. Zin, M. Pylak, T. Wasak, M. Gajda, and Z. Idziaszek, Phys. Rev. A **98**, 051603(R) (2018).

[28] T. Ilg, J. Kumlin, L. Santos, D. S. Petrov, and H. P. Büchler, Phys. Rev. A **98**, 051604(R) (2018).

[29] L. Lavoine and T. Bourdel, Phys. Rev. A **103**, 033312 (2021).

[30] M. Ota and G. E. Astrakharchik, SciPost Phys. **9**, 20 (2020).

[31] L. Parisi and S. Giorgini, Phys. Rev. A **102**, 023318 (2020).

[32] I. Morera, G. E. Astrakharchik, A. Polls, and B. Juliá-Díaz, Phys. Rev. Research **2**, 022008(R) (2020).

[33] I. Morera, B. Juli-Díaz, and M. Valiente, arXiv:2103.16499.

[34] E. Chiquillo, Phys. Rev. A **97**, 013614 (2018).

[35] H. Hu, J. Wang, and X.-J. Liu, Phys. Rev. A **102**, 043301 (2020).

[36] I. Morera, G. E. Astrakharchik, A. Polls, and B. Juliá-Díaz, Phys. Rev. Lett. **126**, 023001 (2021).

[37] A. Cappellaro, T. Macrì, and L. Salasnich, Phys. Rev. A **97**, 053623 (2018).

[38] M. Tylutki, G. E. Astrakharchik, B. A. Malomed, and D. S. Petrov, Phys. Rev. A **101**, 051601(R) (2020).

[39] G. De Rosi, G. E. Astrakharchik, and P. Massignan, Phys. Rev. A **103**, 043316 (2021).

[40] F. Ancilotto, M. Barranco, M. Guilleumas, and M. Pi, Phys. Rev. A **98**, 053623 (2018).

[41] F. Minardi, F. Ancilotto, A. Burchianti, C. D'Errico, C. Fort, and M. Modugno, Phys. Rev. A **100**, 063636 (2019).

[42] S. I. Mistakidis, T. Mithun, P. G. Kevrekidis, H. R. Sadeghpour, and P. Schmelcher, Phys. Rev. Research **3**, 043128 (2021).

[43] T. Mithun, A. Maluckov, K. Kasamatsu, B. A. Malomed, and A. Khare, Symmetry **12**, 174 (2020).

[44] P. Naidon and D. S. Petrov, Phys. Rev. Lett. **126**, 115301 (2021).

[45] F. Bloch, Phys. Rev. A **7**, 2187 (1973).

[46] R. Kanamoto, H. Saito and M. Ueda, Phys. Rev. A **67**, 013608 (2003).

[47] C. Ryu, M. F. Andersen, P. Cladé, V. Natarajan, K. Helmerson, and W. D. Phillips, Phys. Rev. Lett. **99**, 260401 (2007).

[48] A. Ramanathan, K. C. Wright, S. R. Muniz, M. Zelan, W. T. Hill, C. J. Lobb, K. Helmerson, W. D. Phillips, and G. K. Campbell, Phys. Rev. Lett. **106**, 130401 (2011).

[49] K. C. Wright, R. B. Blakestad, C. J. Lobb, W. D. Phillips, and G. K. Campbell, Phys. Rev. Lett. **110**, 025302 (2013).

[50] C. Ryu, P. W. Blackburn, A. A. Blinova, and M. G. Boshier, Phys. Rev. Lett. **111**, 205301 (2013).

[51] S. Beattie, S. Moulder, R. J. Fletcher, and Z. Hadzibabic, Phys. Rev. Lett. **110**, 025301 (2013).

[52] S. Eckel, J. G. Lee, F. Jendrzejewski, N. Murray, C. W. Clark, C. J. Lobb, W. D. Phillips, M. Edwards, and G. K. Campbell, Nature (London) **506**, 200 (2014).

[53] M. Guo and T. Pfau, Front. Phys. **16**, 32202 (2020).

[54] E. Nicolau, J. Mompart, B. Juliá-Díaz, and V. Ahufinger, Phys. Rev. A **102**, 023331 (2020).

[55] J. Smyrnakis, S. Bargi, G. M. Kavoulakis, M. Magiropoulos, K. Kärkkäinen, and S. M. Reimann, Phys. Rev. Lett. **103**, 100404 (2009).

[56] T. Shimodaira, T. Kishimoto and H. Saito, Phys. Rev. A **82**, 013647 (2010).

[57] J. Smyrnakis, M. Magiropoulos, A. D. Jackson, and G. M. Kavoulakis, J. Phys. B: At. Opt. Mol. Phys. **45**, 235302 (2012).

[58] K. Anoshkin, Z. Wu, and E. Zaremba, Phys. Rev. A **88**, 013609 (2013).

[59] J. Smyrnakis, M. Magiropoulos, N. K. Efremidis, and G. M. Kavoulakis, J. Phys. B: At. Opt. Mol. Phys. **47**, 215302 (2014).

[60] M. Abad, A. Sartori, S. Finazzi, and A. Recati, Phys. Rev. A **89**, 053602 (2014).

[61] A. Muñoz Mateo, A. Gallemí, M. Guilleumas, and R. Mayol, Phys. Rev. A **91**, 063625 (2015).

[62] A. Roussou, J. Smyrnakis, M. Magiropoulos, N. K. Efremidis, G. M. Kavoulakis, P. Sandin, M. Ögren, and M. Gulliksson, New J. Phys. **20**, 045006 (2018).

[63] Z. Chen, Y. Li, N. P. Proukakis, and B. A. Malomed, New J. Phys. **21**, 073058 (2019).

[64] J. Polo, R. Dubessy, P. Pedri, H. Perrin, and A. Minguzzi, Phys. Rev. Lett. **123**, 195301 (2019).

[65] M. Ögren, G. Drougakis, G. Vasilakis, W. von Klitzing, and G. M. Kavoulakis, J. Phys. B: At. Opt. Mol. Phys. **54**, 145303 (2021).

[66] S. Giorgini, L.P. Pitaevskii, and S. Stringari, J. Low Temp. Phys. **109**, 309 (1997).

[67] A. R. P. Lima, and A. Pelster, Phys. Rev. A **84**, 041604(R) (2011).

[68] A.R.P. Lima, and A. Pelster, Phys. Rev. A **86**, 063609 (2012).

[69] L. Salasnich, Appl. Sci. **8(10)**, 1998 (2018).

[70] S. Komineas, N. R. Cooper, and N. Papanicolaou, Phys. Rev. A **72**, 053624 (2005).

[71] K. Kärkkäinen, J. Christensson, G. Reinisch, G. M. Kavoulakis, and S. M. Reimann, Phys. Rev. A **76**, 043627 (2007).

[72] M. Nilsson Tengstrand, P. Stürmer, E. Ö. Karabulut, S. M. Reimann, Phys. Rev. Lett. **123**, 160405 (2019).

[73] P. Examilioti and G. Kavoulakis, J. Phys. B: At. Mol. Opt. Phys. **53**, 175301 (2020).

[74] X. Cui and Y. Ma, Phys. Rev. Research **3**, L012027 (2021).

[75] M. N. Tengstrand, D. Boholm, R. Sachdeva, J. Bengtsson, and S. M. Reimann, Phys. Rev. A **103**, 013313 (2021).

[76] S. M. Roccuzzo and F. Ancilotto, Phys. Rev. A **99**, 041601(R) (2019).

[77] A. J. Leggett, Phys. Rev. Lett. **25**, 1543 (1970).

[78] A. J. Leggett, J. Stat. Phys. **93**, 927 (1998).

[79] S. M. Roccuzzo, A. Gallemí, A. Recati, and S. Stringari, Phys. Rev. Lett. **124**, 045702 (2020).

[80] L. Santos, G. V. Shlyapnikov, and M. Lewenstein, Phys. Rev. Lett. **90**, 250403 (2003).

[81] D. Mihalache, D. Mazilu, B. A. Malomed, and F. Lederer, Phys. Rev. A **73**, 043615 (2006).

[82] Y. Li, Z. Chen, Z. Luo, C. Huang, H. Tan, W. Pang, and B. A. Malomed, Phys. Rev. A **98**, 063602 (2018).

[83] Y. Gao and Y. Cai, J. Comput. Phys. **403**, 109058 (2019).

[84] Y. Guo, R. Dubessy, M. D. G. de Herve, A. Kumar, T. Badr, A. Perrin, L. Longchambon, and H. Perrin, Phys. Rev. Lett. **124**, 025301 (2020).

[85] M. de Goër de Herve, Y. Guo, C. D. Rossi, A. Kumar, T. Badr, R. Dubessy, L. Longchambon, and H. Perrin, J. Phys. B: At. Mol. Opt. Phys. **54**, 125302 (2021).